

# Composition variation of illite-vermiculite-smectite mixed-layer minerals in a bentonite bed from Charente (France)

A. MEUNIER<sup>1,\*</sup>, B. LANSON<sup>2</sup> AND B. VELDE<sup>3</sup>

<sup>1</sup>HYDRASA UMR 6532, CNRS-University of Poitiers, 40 av. Recteur Pineau, 86022 Poitiers Cedex, <sup>2</sup>LGIT – Maison des GéoSciences, CNRS - University Joseph Fourier, PO Box 53, 38041 Grenoble Cedex 9, and <sup>3</sup>Laboratoire de Géologie, E.N.S., 24 rue Lhomond, 75231 Paris Cedex 05, France

(Received 18 June 2003; revised 9 February 2004)

**ABSTRACT:** Mineralogical and chemical variations were studied in the upper half of a 1 m thick discontinuous bentonite bed interlaminated in the Lower Cenomanian sedimentary formations of the northern Aquitaine basin (France). X-ray diffraction patterns obtained from the <2 µm fraction in the Ca and K-saturated states were decomposed and compared to those calculated from decomposition parameters. They revealed the presence of two highly expandable illite-expandable (I-Exp) mixed-layer minerals (MLMs). The relative proportions of the two MLMs evolve steadily with depth leading to the decrease of the cation exchange capacity and of the (Na + Ca) content towards the centre of the bentonite bed. However, the system is essentially isochemical and Mg, Al, Si, K and Fe are roughly constant in the bulk samples. It is thought that the mineralogical zonation results from the initial stages of the smectite formation in an ash layer.

In the Ca-saturated state, the expandable component of these MLMs was for the most part homogeneous with the presence of 2 sheets of ethylene glycol molecules in the interlayer. However, the heterogeneous hydration behaviour of these expandable layers was enhanced by the K-saturation test. From this test, the presence of three layer types with contrasting layer charge was evidenced from their contrasting swelling abilities. The C<sub>12</sub>-alkylammonium saturation test applied to samples in which the octahedral charge had previously been neutralized (Hofmann-Klemen treatment) showed that the tetrahedral charge is located on specific layers. These layers are responsible for the heterogeneous hydration behaviour. Low-charge smectite layers are mostly octahedrally substituted, whereas for intermediate- and high-charge layers this montmorillonitic charge is complemented by additional tetrahedral substitutions (0.30 and 0.35–0.40 charge per O<sub>10</sub>(OH)<sub>2</sub>, respectively).

**KEYWORDS:** bentonite, Charente, France, decomposition, high-charge smectite, hydration properties, mixed-layer minerals, XRD.

It has been established in numerous studies that smectitic bentonite beds tend to alter to illite by diffusion processes at their contacts with encompassing rocks and sediments (Foscolos & Kodama, 1974; Hoffman & Hower, 1979; Huff & Türkmenoglu, 1981; Velde & Brusewitz, 1982;

Altaner *et al.*, 1984). These sedimentary units form K-bentonites. The rate at which this diffusion-controlled reaction occurs has been estimated by Altaner (1985). The most remarkable observation is the increase of the K content in the essentially monomineralic bed towards its outer edge. In most cases, illite-smectite (I-S) mixed-layer minerals (MLMs) are smectite-rich in the interior of the bentonite bed and have a higher illite content at the edge. Such occurrences have been assumed to

\* E-mail: alain.meunier@hydrasa.univ-poitiers.fr  
DOI: 10.1180/0009855043930137

represent simple smectite-to-illite reaction series which appear to differ in their kinetics of transformation when compared to detrital shales (Šuchá *et al.*, 1993).

Implicit in such a mineralogical sequence is the initial conversion of the acidic volcanic ash into a monomineralic material of essentially pure smectite composition. In this preliminary process, a chemical exchange with the exterior of the ash bed is necessary to transform the original volcanic rock into smectite through a non-isochemical process. It is always assumed that the initial ash bed transformation gives an homogeneous smectite layer (Altaner, 1985). However, since the initial phases of the ash-to-clay transformation imply an exchange of several elements, there is little reason to exclude an initial composition gradient during the smectite formation process.

The object of the present investigation is to assess the mineralogical homogeneity of a Cretaceous bentonite bed which has experienced little burial diagenesis leading to clay mineral transformation. The unit has experienced only shallow burial and no tectonic effect during its 120 Ma existence (Meunier *et al.*, 1999). Here, we expect to see the initial stages of diffusion and smectite formation before illitization (Meunier *et al.*, 2000).

## MATERIALS AND METHODS

### Sample location and existing data

The investigated bentonite bed is discontinuously interlaminated in the Lower Cenomanian sedimentary formations from the northern Aquitaine basin (Fig. 1). It belongs to the A unit in the Lower Cretaceous stratigraphic sequence (Meunier *et al.*, 1999). This bed is 1 m thick in the sampling area: a quarry near Archingeay (Charente, France). There, it is interlaminated between two unconsolidated sand deposits (Fig. 1). For this study, five samples were taken out at regular 10 cm intervals and indexed A, B, C, D and E from top to bottom in a vertical profile.

### Analytical procedures

All samples were crushed gently in an agate mortar. The powders were then dispersed ultrasonically in distilled water and the  $<2 \mu\text{m}$  fraction was separated from the suspension using standard

sedimentation procedures. Oriented preparations of a Ca-saturated  $<2 \mu\text{m}$  fraction were analysed by means of X-ray diffraction (XRD) in the air-dried (AD) state, and after ethylene glycol (EG) solvation. Additional analyses were carried out from EG-solvated samples after K-saturation, and after Li-exchange and heating to 300°C (Li-300; Hofmann & Klemen, 1950). The contribution of tetrahedral substitutions to the total layer charge was estimated by comparing XRD patterns obtained for each sample after saturation with  $\text{C}_{12}$ -alkylammonium (Olis *et al.*, 1990) of the original sample and of the Li-300 sample in which the octahedral charge has been neutralized. The XRD patterns were recorded using a Philips® PW 1730 diffractometer (Ni-filtered  $\text{Cu-K}\alpha$  radiation generated at 40 kV and 40 mA), equipped with a stepping motor drive in the goniometer

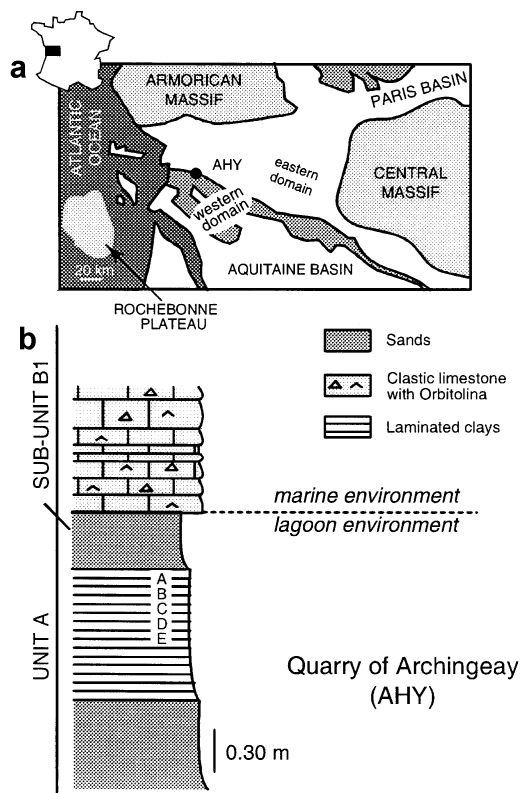


FIG. 1. Geological settings. (a) Location of the Archingeay quarry (AHY) in the Cenomanian formations of the northern part of the Aquitaine basin. (b) Geological sequence and sampling of the bentonite bed (A to E).

(SOCABIM DACO system). A Co-K $\alpha$  radiation generated at 40 kV and 40 mA has been used to analyse the samples saturated with C<sub>12</sub>-alkylammonium ions. The usual analytical conditions were 2–35°2 $\theta$  as the data collection range, a scanning step size of 0.025°2 $\theta$  and a counting time of 6 s per step.

The smectite samples were analysed chemically for major elements using ICP-AES (experimental errors are <1% for SiO<sub>2</sub>, Al<sub>2</sub>O<sub>3</sub>, Fe<sub>2</sub>O<sub>3</sub>, MgO; <2% for TiO<sub>2</sub>, MnO, CaO, K<sub>2</sub>O, Na<sub>2</sub>O). The cation exchange capacity (CEC) was obtained by saturation with Mg<sup>2+</sup>, the excess Mg salt being carefully washed out with ethanol. The Mg<sup>2+</sup> was then displaced by NH<sub>4</sub><sup>+</sup> and analysed by atomic absorption spectroscopy (AAS) in the exchange solution (experimental error <1% for CEC >60 cmol kg<sup>-1</sup>).

#### Methods for the interpretation of XRD patterns

Most identification methods routinely used to determine the composition of I-S MLMs rely on the position of diffraction maxima, on relative positions of maxima, on intensity ratios between these bands, or on peak/background intensity ratios (Środoń, 1981; Velde *et al.*, 1986; Watanabe, 1988; Inoue *et al.*, 1989; Esposito & Whitney, 1995; amongst many others). These parameters are first measured on experimental XRD patterns and then compared with values determined from calculated patterns. However, one may note that all these methods rely on two main hypotheses: (1) the expandable (inter)layers are assumed to be homogeneous as all calculations are performed for 2 components: illite and expandable layers (I-Exp). As a consequence, none of these identification methods allows the description of three-component systems such as the illite-smectite-vermiculite (I-S-V) MLMs reported (e.g.) by Drits *et al.* (1997) in which the expandable layers exhibit heterogeneous behaviour after hydration and/or EG solvation and are differentiated as smectite (S-type, fully expandable layers with 2 sheets of H<sub>2</sub>O or EG molecules) and vermiculite (V-type, partly expandable layers with only 1 sheet of H<sub>2</sub>O or EG molecules; see Meunier *et al.*, 2000 for detailed definitions); (2) samples are most often assumed to be monomineralic and these methods may rarely be satisfactorily applied to samples containing several MLMs.

The errors introduced by these methods when applied to three-component systems may be illustrated by applying some of them to XRD patterns calculated for 20:80 I-Exp MLMs in which the swelling behaviour of the expandable layers is

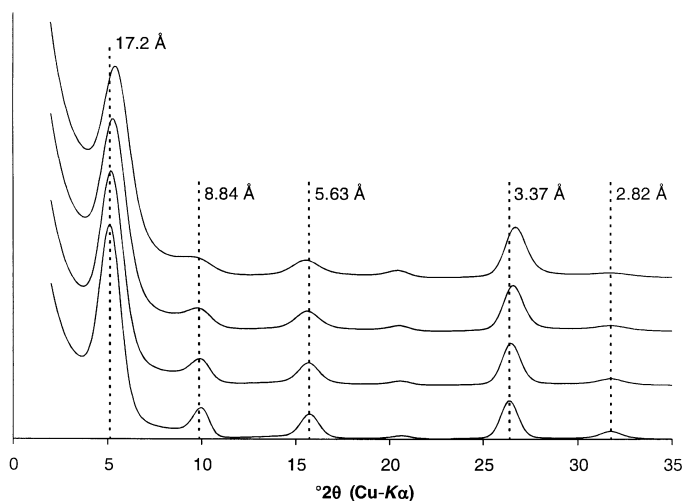


FIG. 2. XRD patterns calculated for randomly interstratified illite-expandable (I-Exp) mixed-layer minerals (MLMs). The proportion of expandable layers (80%) is constant for all patterns but the swelling behaviour is modified. From top to bottom the relative proportion of expandable layers accepting two sheets of ethylene glycol (EG) molecules in their interlayers (S-type layers) increases by 50–80%. Structural parameters (ion position,  $d$  spacings) used for the calculation are those recommended by Moore & Reynolds (1989).

TABLE 1. Comparison of the results given by different identification methods from saddle/peak ratio or peak positions of calculated XRD patterns of three component mixed-layer minerals. NA: not analysed. (See text for details).

$I_{20\%}-Exp_{80\%}$		Peak position ( $2\theta$ Cu- $K\alpha$ )					Identification
$^3S\%$	$^4V\%$	$^1001$	$^1002$	$^1003$	$^1005$	$^1006$	Środoń (1981)
80	0	5.11 17.3 Å	9.96 8.88 Å	15.73 5.63 Å	26.40 3.376 Å	31.75 2.818 Å	90%S
70	10	5.18 17.0 Å	9.89 8.94 Å	15.69 5.65 Å	26.48 3.366 Å	31.74 2.819 Å	95%S
60	20	5.28 16.7 Å	9.77 9.05 Å	15.62 5.67 Å	26.59 3.352 Å	31.73 2.820 Å	NA
50	30	5.40 16.4 Å	9.33 9.48 Å	15.54 5.70 Å	26.73 3.335 Å	31.69 2.823 Å	NA

<sup>1</sup> Peaks are labelled as smectite; <sup>2</sup> randomly ordered illite-smectite mixed-layer mineral; <sup>3</sup> S: smectite (2 EG sheets), <sup>4</sup> V: vermiculite (1 EG sheet)

$I_{20\%}-Exp_{80\%}$		Peak position	Saddle/peak ratio	Identification	
S%	V%			Inoue <i>et al.</i> (1989)	Weir <i>et al.</i> (1975)
80	0	5.11 17.3 Å	0.38	72%	82%
70	10	5.18 17.0 Å	0.45	67%	78%
60	20	5.28 16.7 Å	0.53	62%	74%
50	30	5.40 16.4 Å	0.60	57%	72%

heterogeneous (Fig. 2). Initially, one may note in Table 1 that the identification results obtained for a simple two-component system (0%V in I-S) depend strongly on the identification method used as estimates range from 90 to 72% smectite. In addition, the identification results also depend on the swelling behaviour of the expandable layers. Some of the identification methods used are not applicable if V-type layers are present in I-Exp MLMs, whereas others may still be applied but provide different results as a function of the relative proportions of S- and V-type layers in the stacking sequences, increasing the range for the estimated smectite content to 95–54% (Table 1).

Because the presence of expandable layers with contrasting swelling behaviours may also be encountered in bentonites (Calarge *et al.*, 2003) a three-step process was adopted to identify the MLMs present in our bentonite samples: first, decomposition of the diffraction peaks into Gaussian and Lorentzian elementary contributions

was performed using the DECOMPXR program (Lanson, 1997). This decomposition procedure was carried out on 00 $l$  peaks from XRD patterns recorded after different sample treatments (Ca-AD, Ca-EG, K-EG of peaks at 15–20, 8–12 and 2–12 $2\theta$  Cu- $K\alpha$  angular ranges, respectively). Special attention was paid to the first steps of the procedure, and specifically to background stripping. As recommended by Lanson (1997) the background was assumed to be linear whenever possible ( $2\theta \geq \sim 8^\circ$ ), and interpolated assuming a Lorentz factor-like shape in low-angle regions. The decomposition was performed by obtaining a satisfactory fit to the experimental data using a minimum number of elementary contributions. However, these elementary contributions are related to specific (sub-) populations of crystals which contribute to the scattered intensity over the whole angular range whatever the physical and chemical pre-treatment. As a consequence, the preliminary identification allowed us to introduce additional constraints on the

number of elementary contributions that can be used in the analysis of smectite patterns following the different treatments. In the present case, constraints were not only derived from the processing of peaks from the same XRD pattern but also from the analysis of peaks from patterns of the same sample recorded in different conditions (cation exchange, EG solvation, etc.) as recommended by Drits *et al.* (1997) and Sakharov *et al.* (1999) for their multi-specimen approach.

The decomposition allowed an objective description of peak profile modification with 'depth' in the bentonite bed. Second, the position, intensity and FWHM parameters of these elementary contributions were used for a preliminary individual identification of each 'clay phase' (type of MLM; % smectite) by comparison with calculated patterns. The XRD patterns were calculated using the programs by Plançon & Drits (2000; <http://www.univ-orleans.fr/ESEM/plancon>) which allow the calculation of three-component MLMs without restrictions on the nature of the different layer types or on the junction probabilities. All parameters necessary for such calculations (atomic positions, *d* spacings) were set as recommended by Moore & Reynolds (1989) except for the basal spacing of smectite layers with only one sheet of EG molecules which was set to 13.5 Å. Finally, the validity of this preliminary identification was checked by the calculation of the complete XRD profile corresponding to the various elementary contributions identified.

## RESULTS

### *Chemical composition*

The chemical compositions of the <2 µm size fraction from the five samples (Table 2) are relatively homogeneous in spite of some erratic variations related to impurities. The SiO<sub>2</sub> content varies because of the presence of microcrystalline quartz (e.g. sample D). The amounts of CaO and Na<sub>2</sub>O as well as the CEC decrease regularly with increasing depth (Fig. 3) while the K<sub>2</sub>O content remains roughly constant throughout the bed.

### *XRD analyses*

*Air-dried and glycol-solvated states (Ca-saturated).* According to Inoue *et al.* (1989), the low background intensity on the low-angle side of the

smectite 001 reflection suggests a high smectite content in the investigated clays (Figs 4, 5). However, on the same experimental pattern the significant asymmetry of the smectite 002 reflection (~8.55 Å) towards lower angles (Fig. 4) suggests the presence of several expandable phases. If this asymmetry was due to contrasting swelling ability of expandable layers, a significant shift of the ~17.0 Å reflection would also be observed as illustrated in Fig. 2. The presence of these highly expandable MLMs is also proven by the asymmetry of the smectite 003 reflection at ~5.00 Å in the Ca-saturated AD pattern (Fig. 5), whereas a sharp symmetrical peak is usually observed when essentially expandable phases are contributing to the diffracted intensity even if the hydration state of the expandable layers is not homogeneous. The above peak asymmetries seem to evolve with depth in the sampled sequence (Figs 4, 5) to indicate a change in the composition of MLMs, which could be related to the CEC evolution with depth in the sampled sequence.

To assess the possible presence of such different MLMs, and to obtain an objective description of their diffraction behaviour, we have decomposed the peaks mentioned above. It was first assumed that all mixed-layer components, and illite, make a unique contribution in each of these angular ranges. The validity of this assumption was checked in the identification step by the calculation of the whole experimental XRD profile. All experimental XRD patterns were successfully fitted with three contri-

TABLE 2. Chemical composition and CEC of the <2 µm fraction of smectite collected at several points in the bentonite layer.

Sample	A	B	C	D	E
Sampling depth (cm)	10	20	30	40	50
SiO <sub>2</sub>	57.78	57.03	56.36	62.22	57.08
Al <sub>2</sub> O <sub>3</sub>	15.63	16.04	16.09	14.41	15.82
Fe <sub>2</sub> O <sub>3</sub>	4.46	5.37	5.00	4.13	3.91
MgO	1.99	2.03	1.95	1.67	1.74
TiO <sub>2</sub>	0.82	0.85	0.96	0.84	0.88
MnO	0.01	0.01	0.01	0.01	0.01
CaO	3.35	2.18	1.44	1.40	1.16
Na <sub>2</sub> O	0.31	0.23	0.18	0.16	0.11
K <sub>2</sub> O	1.31	1.31	1.29	1.36	1.29
CEC (cmol kg <sup>-1</sup> )	79.8	78.8	76.3	75.7	74.1

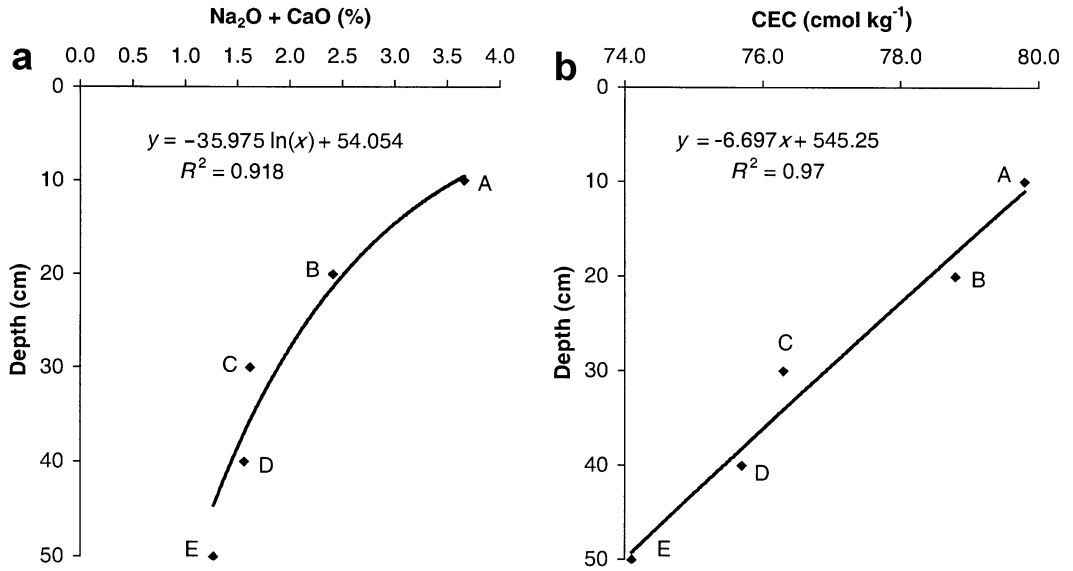


FIG. 3. Variation of the  $\text{Na}_2\text{O}+\text{CaO}$  amounts (a) and the CEC ( $\text{cmol kg}^{-1}$ ) (b) from the edge (A) to centre (E) of the bentonite bed.

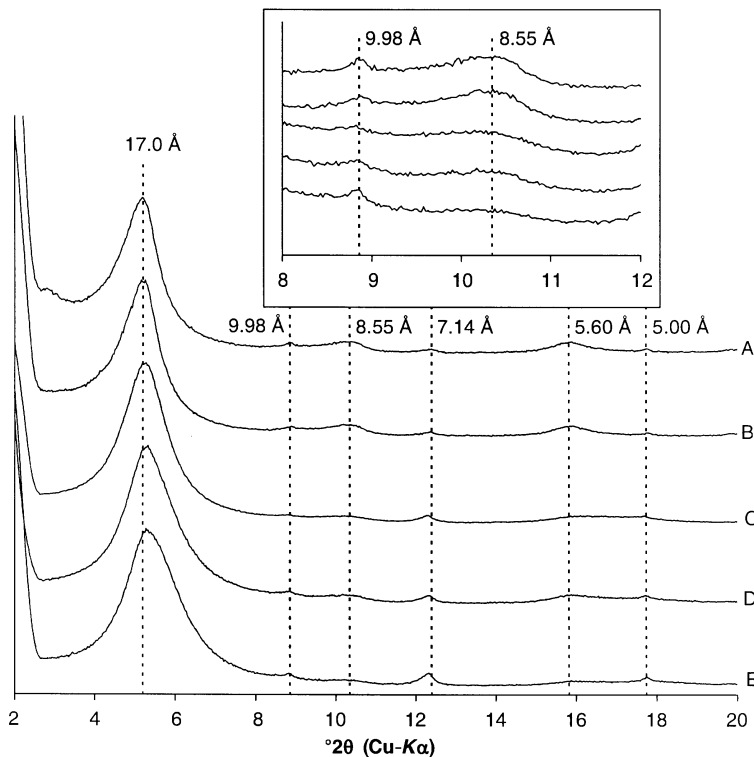


FIG. 4. XRD patterns of oriented preparations from the Ca-saturated samples in the ethylene glycol-saturated state (EG). Inset are details of the XRD patterns in the 8–12°  $2\theta$   $\text{Cu-K}\alpha$  angular range. The positions of the 002 diffraction peaks remain constant while their shape and intensity vary with depth.

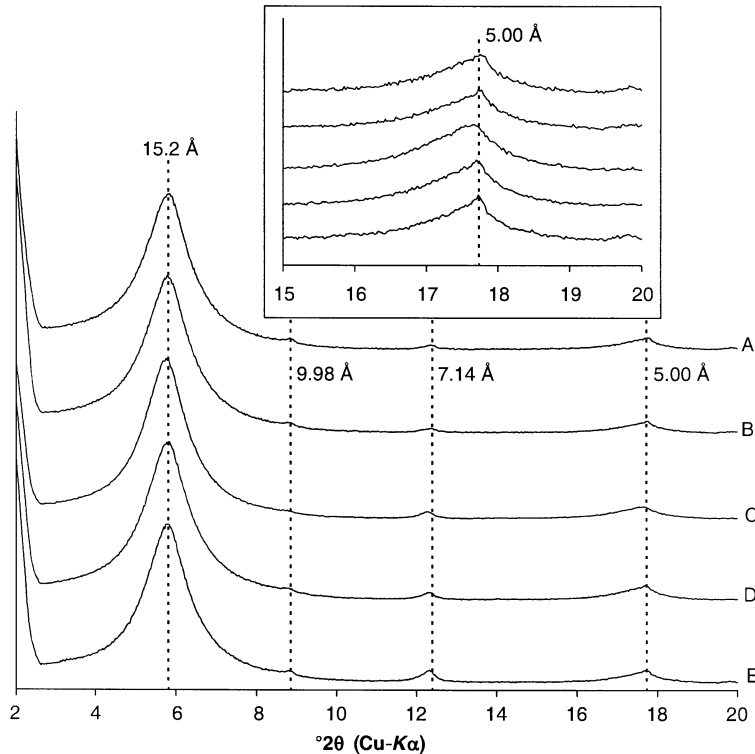


FIG. 5. XRD patterns of oriented preparations from the Ca-saturated samples in the air-dried (AD) state. Inset are the details of the XRD patterns in the 15–20°2 $\theta$  Cu-K $\alpha$  angular range. The positions of the 003 diffraction peaks remain constant while their shape and intensity vary with depth.

butions. The sharper contribution (FWHM = 0.2–0.5°2 $\theta$ ) probably corresponds to illite and/or detrital mica whereas the other two phases exhibit broader reflections of variable intensities and positions (Tables 3, 4; Figs 6, 7). For the Ca-EG diffraction pattern, the positions of these two contributions range from 8.45 to 8.52 Å (major contribution) and from 8.72 to 9.22 Å, respectively

(Table 3; Fig. 6). These two mixed-layered structures contribute to the Ca-AD XRD pattern at 4.99–5.03 Å, and 5.03–5.07 Å, respectively (Table 4; Fig. 7). These contributions were both attributed to I-Exp MLMs.

To check the validity of the assumed nature of phases contributing to the diffracted intensity, experimental XRD patterns were compared to

TABLE 3. Decomposition values of XRD patterns (8 to 12°2 $\theta$  Cu-K $\alpha$  angular range) of bentonite samples in the Ca-saturated EG state.

Sample	<sup>1</sup> I-Exp <sub>1</sub>			<sup>1</sup> I-Exp <sub>2</sub>			Illite		
	<sup>2</sup> Pos. (Å)	Intensity	<sup>3</sup> FWHM	<sup>2</sup> Pos. (Å)	Intensity	<sup>3</sup> FWHM	<sup>2</sup> Pos. (Å)	Intensity	<sup>3</sup> FWHM
A	8.52	397	0.76	9.26	216	1.46	9.96	217	0.22
B	8.52	559	0.78	9.23	275	1.26	9.99	209	0.38
C	8.49	315	0.72	8.97	153	0.70	10.02	128	0.29
D	8.43	204	0.59	8.75	276	1.03	10.02	272	0.50
E	8.47	113	0.67	8.72	93	1.11	10.02	318	0.30

<sup>1</sup> I-S MLMs; <sup>2</sup> peak position; <sup>3</sup> full width at half maximum intensity

TABLE 4. Decomposition values of XRD patterns (15 to 20°2 $\theta$  Cu-K $\alpha$  angular range) of bentonite samples in the Ca-saturated AD state.

Sample	<sup>1</sup> I-Exp <sub>1</sub> ± Illite			<sup>1</sup> I-Exp <sub>2</sub>			Illite		
	<sup>2</sup> Pos. (Å)	Intensity	<sup>3</sup> FWHM	<sup>2</sup> Pos. (Å)	Intensity	<sup>3</sup> FWHM	<sup>2</sup> Pos. (Å)	Intensity	<sup>3</sup> FWHM
A	4.99	249	0.57	5.03	368	1.47	4.95	189	0.17
B	5.00	329	0.74	5.04	366	1.62	4.96	251	0.20
C	5.03	581	0.95	5.07	616	1.89	4.99	364	0.36
D	5.00	515	0.74	5.07	631	1.71	4.97	344	0.19
E	5.00	393	0.67	5.06	446	1.72	4.97	339	0.17

<sup>1</sup> I-S MLMs; <sup>2</sup> peak position; <sup>3</sup> full width at half maximum intensity

profiles calculated with the programs developed by Plançon & Drits (2000). It was possible to obtain a satisfactory fit to the experimental data by assuming, in agreement with the decomposition results, the presence of two MLMs, in addition to an illite-rich phase (Fig. 8). The first mixed-layered structure (I-Exp<sub>1</sub>) corresponds to a highly expandable, disordered (R = 0) I-Exp MLM (peak at ~8.5 Å on the Ca-EG pattern) whereas the second MLM (I-Exp<sub>2</sub>) is less expandable (peak at ~8.9 Å on the Ca-EG pattern). In these two MLMs, the swelling behaviour of the expandable component is heterogeneous as the compositions of I-Exp<sub>1</sub> and I-Exp<sub>2</sub> are 70:20:10 and 40:30:30 (S:V:I ratios), respectively. Because these two MLMs were identified systematically after different sample treatments (see below), no attempt was made to try to describe these two MLMs as a unique MLM.

One may note that the decomposition of Ca-AD XRD patterns leads to intensity ratios between the different contributions that are similar for all samples. On the contrary, the contribution of illite and/or detrital mica is much enhanced on the Ca-EG XRD patterns of samples D and E, as compared to samples A–C, whereas the contribution of I-Exp<sub>1</sub> is decreased for the former samples. This is probably due to the increased contribution of illite crystallites with small coherent scattering domain sizes (CSDS) for samples D and E as shown by the increased breadth of the ~10.0 Å diffraction maximum in the Ca-EG XRD pattern (Fig. 6). On the Ca-AD XRD patterns, the breadth of the diffraction maximum attributed to the illite and/or detrital mica is systematically low (Fig. 7). It is thus likely that this peak represents the whole contribution for illite and/or detrital mica in samples A–C, whereas it accounts only for the larger crystallites in samples D and E. In the Ca-EG

state (Fig. 7) illite crystallites with a smaller CSDS present in samples D and E are included in the I-Exp<sub>1</sub> contribution which is thus enhanced compared to the Ca-AD state (Fig. 6).

#### Identification of smectite layer components

*Hofmann-Klemen treatment.* Following the Hofmann-Klemen treatment, all samples show two broad bands at ~17 Å and 9.6 Å (Fig. 9) corresponding to domains containing mostly expanded beidellitic layers and collapsed montmorillonitic layers, respectively. However, the high saddle/peak ratio observed for the 17 Å peak is reminiscent of the interstratification effects described by Inoue *et al.* (1989) for I-S MLMs and possibly indicates the coexistence (interstratification) of collapsed and expanded layers in the same ‘crystals’. From their similar respective intensities, and considering the greater contribution of the structure and Lorentz-polarization factors to intensity at low angles, the relative abundance of the 17 Å component appears to be lower than that of the 9.60 Å one.

*K-saturated ethylene glycol-solvated state.* The XRD patterns obtained from K-saturated samples in the EG state all exhibit a broad maximum in the 17 Å region (Fig. 10). If compared to the 17 Å band in the Ca-EG sample (Fig. 4), the width of this 17 Å band is considerably increased and its position for A and B samples is shifted towards lower *d* values. This may indicate that the average CSDS is lower in the K-EG state, but a significant decrease of the CSDS would induce a strong shift of the position towards higher *d* values. Rather, this increased peak width is probably related to the presence of layers that are fully expandable after Ca-saturation (S-type) and only partly expandable (V-type) or even collapsed to 10 Å when

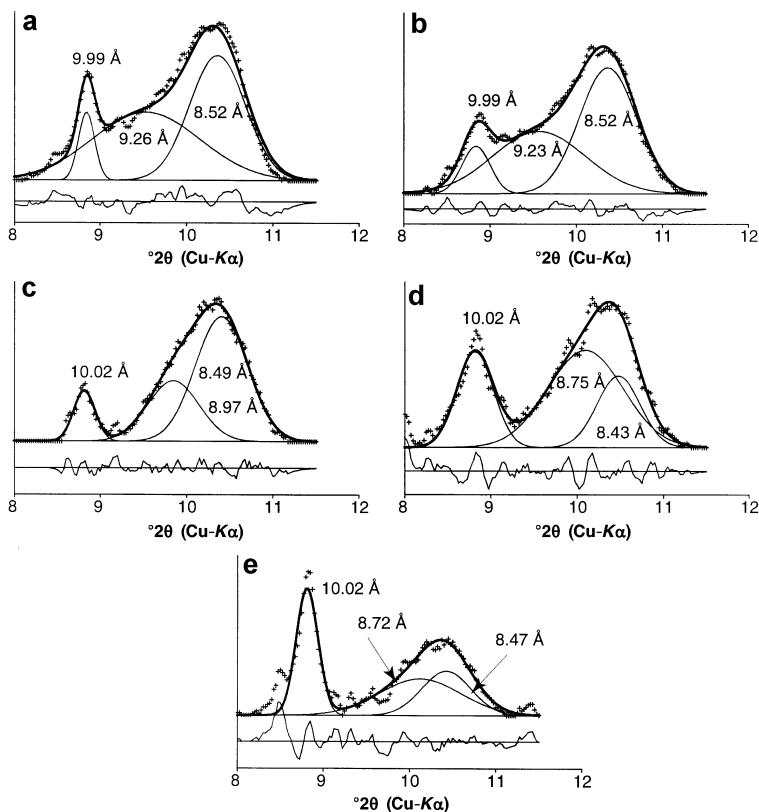


Fig. 6. XRD patterns from Ca-saturated EG samples. Decomposition of the 8–12°2 $\theta$  Cu-K $\alpha$  angular range.

K-saturated. As a result, the peak position shifts towards lower  $d$  values (from 17.06 to 16.12 Å for sample A in the in the Ca-EG and K-EG states, respectively). Since the position shift decreases A to E, the relative proportion of such partly expandable layers probably decreases with depth. The K-saturation outlines the charge heterogeneity of expandable layers in the main smectite-rich I-Exp<sub>1</sub> MLM.

The decomposition of the diffraction profile over 2–12°2 $\theta$  gives a satisfying fit with three diffraction bands (Fig. 11). The overwhelming broad (2.28>FWHM>1.86) 16.22–17.03 Å band represents the sole contribution of the I-Exp<sub>1</sub> phase identified in Ca-saturated samples. The sharp (0.21>FWHM>0.18) contribution at 9.95–10.07 Å is related to the illite/mica phase, whereas the broad (2.32>FWHM>1.87) 10.17–9.82 Å contribution is probably related to the I-Exp<sub>2</sub> mixed-layer structure. The intensity of the latter contribution is extremely low as compared to that attributed to

I-Exp<sub>1</sub>. This contrast probably arises from their contrasting structure factors over this angular range rather than from their relative proportions. In spite of this low intensity, the I-Exp<sub>2</sub> contribution probably integrates the second order of the I-Exp<sub>1</sub> contribution. This is supported by the variability of the I-Exp<sub>2</sub> peak position, and more especially by its shift on the high-angle side of the illite contribution which can hardly be accounted for otherwise.

*C*<sub>12</sub>-alkylammonium saturation state. This study was performed after neutralizing the octahedral charge with the Hofmann-Klemen treatment, which produced collapsed and expandable layers, possibly intratratified (see the Hofmann-Klemen paragraph above). Then, the remaining tetrahedral charge was investigated using the C<sub>12</sub>-alkylammonium saturation procedure to identify high- and low-charge layers (2 or 1 alkylammonium layers, respectively). The resulting XRD patterns show an intense peak at ~13.6 Å which is typical of low-charge layers, which intercalate only one sheet of alkylammonium

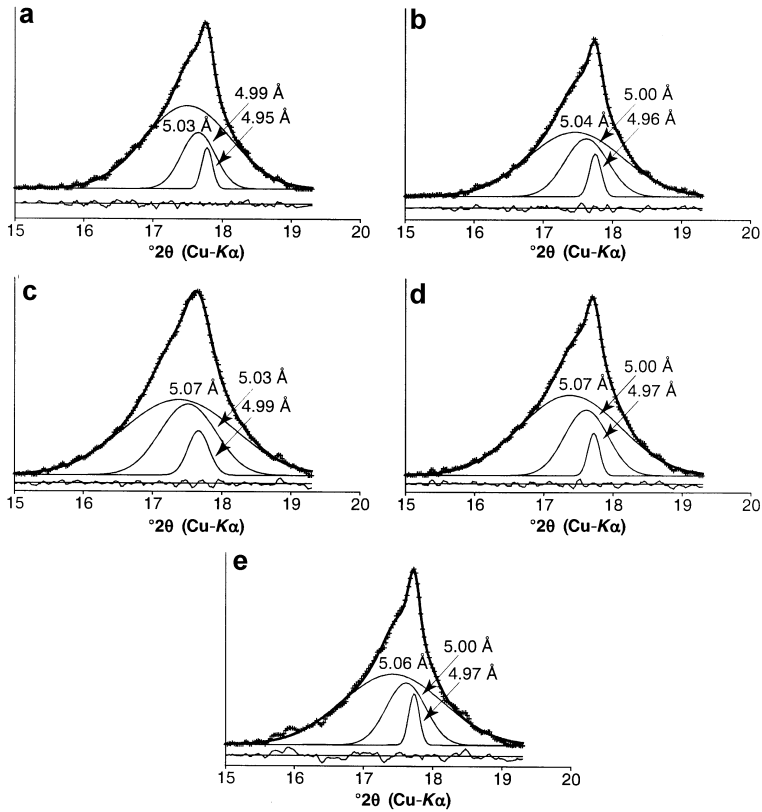


FIG. 7. XRD patterns from Ca-saturated AD samples. Decomposition of the 15–20°2 $\theta$  Cu- $K\alpha$  angular range.

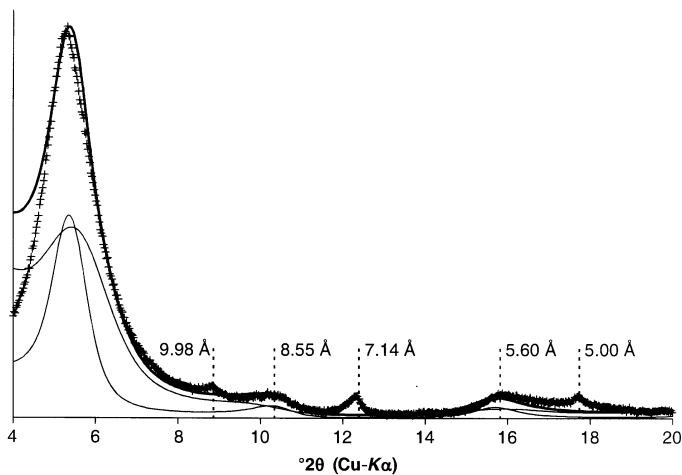


FIG. 8. Calculated XRD patterns from sample D in the Ca-saturated EG state (heavy line) based on the two mixed-layer components determined by the decomposition of the 8–12°2 $\theta$  Cu- $K\alpha$  region. The crosses correspond to the experimental pattern. Mica and kaolinite contributions were calculated but are not included in the figure for simplicity.

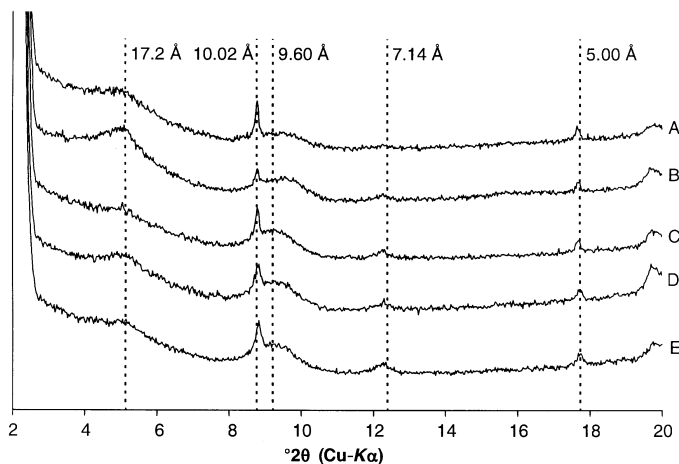


FIG. 9. XRD patterns from oriented mounts in which the octahedral charge has been neutralized using the Hofmann-Klemen treatment.

cations (Lagaly & Weiss, 1969). On the low-angle side of this broad maximum, a shoulder is visible at 17.2 Å indicating the presence of high-charge layers with two sheets of alkylammonium cations. A weak 10 Å peak is also visible on these patterns (Fig. 12). After decomposition, the broad 13.6 Å peak is shown to include the contributions from three different populations of crystals which scatter X-rays coherently (Fig. 13). The main 13.5–13.6 Å peak is typical of low-charge layers having one sheet of alkylammonium cations whereas the 17.1–16.5 Å and the 11.9–11.5 Å peaks probably represent the contributions of domains in which layers with contrasting alkylammonium contents are

interstratified. The first of these contributions (MLM1) includes layers having two and one sheets of alkylammonium cations (high and low tetrahedral charge), respectively, whereas the other contribution (MLM2) includes layers with one and zero alkylammonium sheets (low and no tetrahedral charge), respectively.

## DISCUSSION

Decomposition of the XRD patterns obtained from our samples after different treatments indicates the systematic presence of two (I-Exp) MLMs the structural variability of which contributes to a

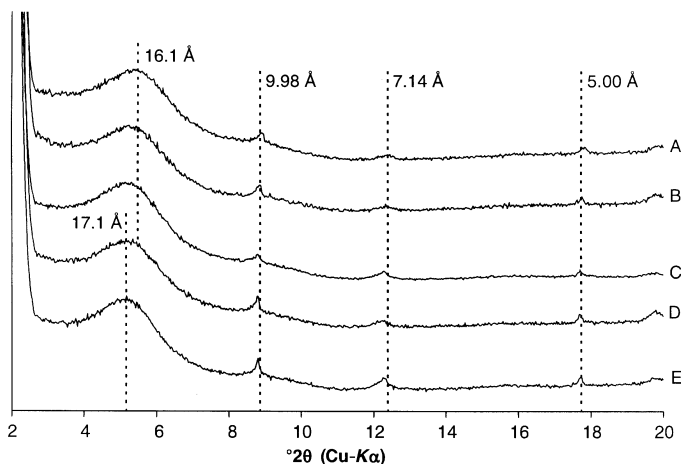


FIG. 10. XRD patterns from oriented preparations of K-saturated samples in the EG state.

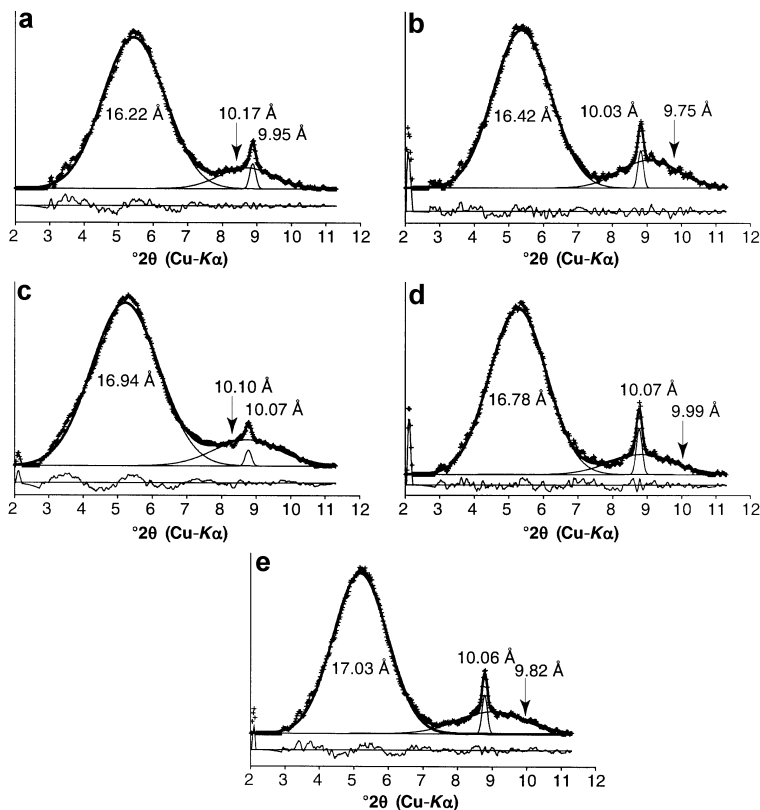


FIG. 11. XRD patterns from K-saturated EG samples. Decomposition of the 2–12°2θ Cu-K $\alpha$  angular range.

general change in XRD profiles. The following discussion will first focus on the characterization of layer-charge heterogeneity (amount and location), and then try to relate the observed evolution of this heterogeneity to the main trends derived from bulk chemical analysis of the clay fraction.

#### Layer-charge heterogeneity

From the comparison of XRD patterns obtained from Ca-EG and K-EG samples, it is possible to hypothesize the coexistence of expandable layers having contrasting charges and hydration properties. The K<sup>+</sup>-for-Ca<sup>2+</sup> exchange increases the number of partly or completely collapsed layers (13 and 10 Å, respectively) in the I-Exp MLMs after EG solvation. For the most expandable I-Exp<sub>1</sub> MLM, this induces a shift of the 17 Å peak towards lower *d* spacing values. In our series of samples, the peak position shifts from 16.22 (sample A) to 17.02 Å (sample E) with depth (Fig. 14) indicating that the

proportion of partly or completely collapsed layers in I-Exp<sub>1</sub> increases from E to A, i.e. towards the outside of the bentonite bed.

From the variation of layer expandability as a function of the interlayer cation, one can define at least three types of expandable layers in the studied samples: (1) low-charge smectite layers that accept two sheets of EG molecules ( $d_{001} \approx 17$  Å) in both Ca- and K-saturated states; (2) intermediate-charge smectite layers accepting two sheets of EG molecules if Ca-saturated but only one ( $d_{001} \approx 13$  Å) when K-saturated; (3) high-charge layers (vermiculite) that accept 1 sheet of EG molecules when Ca-saturated and are collapsed ( $d_{001} \approx 10$  Å) when K-saturated.

From the presence of domains containing mostly expanded beidellitic layers and collapsed montmorillonitic layers after the Hofmann-Klemen treatment, it is possible to evaluate the relative contributions of octahedral and tetrahedral substitutions to the total layer charge shown by Cuadros &

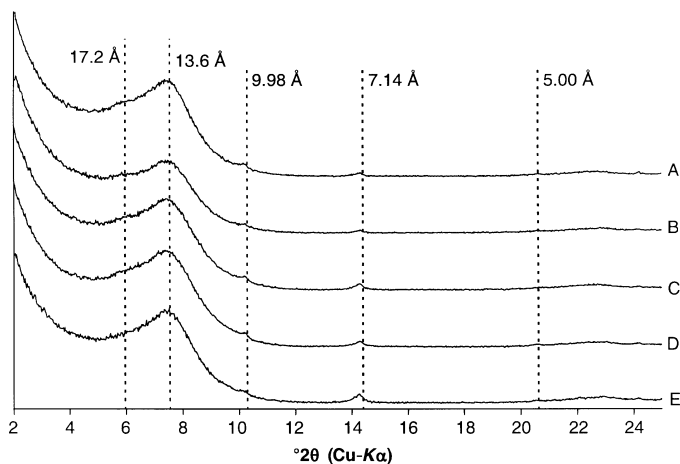


FIG. 12. XRD patterns from  $C_{12}$ -alkylammonium-saturated samples (Co-K $\alpha$ ) in which the octahedral charge has previously been neutralized using the Hofmann-Klemen treatment.

Altaner (1998) in smectitic minerals from bentonite deposits. First of all, one may note the much greater

contribution of octahedral substitutions as demonstrated by the similar intensities of the 9.6 and 17 Å

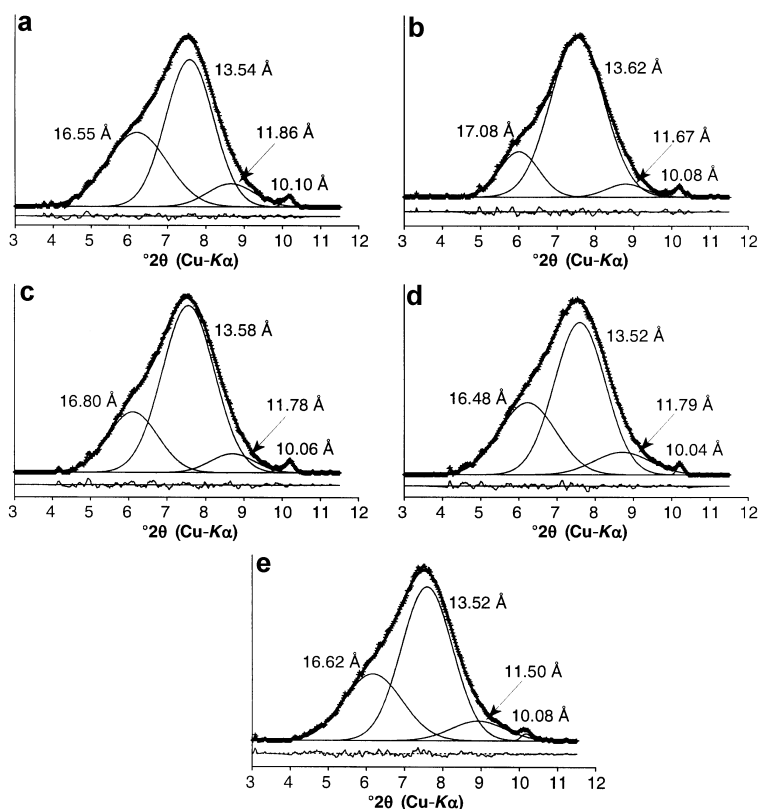


FIG. 13. XRD patterns from Li-saturated samples heated to 300°C and saturated with a  $C_{12}$  alkylammonium. Decomposition of the 3–12 $^{\circ}2\theta$  Co-K $\alpha$  angular range.

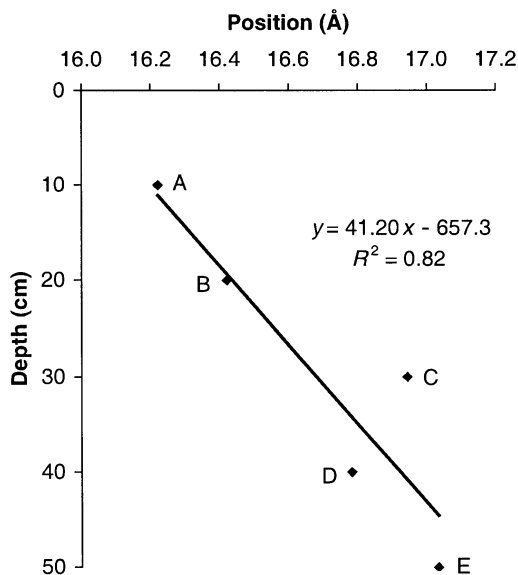


FIG. 14. Variation of the position of the most intense band in decomposed XRD patterns from K-saturated samples with depth. The lower the position, the higher the high-charge layer amount (see text for details).

peaks observed on XRD patterns recorded after the Hofmann-Klemen treatment (Fig. 9). As a consequence, expandability possibly depends on the amount of beidellitic substitution. The  $C_{12}$ -alkylammonium saturation of samples previously submitted to the Hofmann-Klemen treatment to neutralize their octahedral charge allows one to analyse further this beidellitic charge.

Decomposition of these XRD patterns shows that the 13.6 Å band (one sheet of alkylammonium cations) is the most intense, indicating that, in most of the layers with tetrahedral substitutions, these represent only  $\sim 0.30$  charge per  $O_{10}(OH)_2$  (Olis *et al.*, 1990). The presence of the 16.5–17.1 Å shoulder (two sheets of alkylammonium cations) shows that some expandable layers present a higher tetrahedral charge (0.35 to 0.40 per  $O_{10}(OH)_2$ ). The amounts of  $Al_2O_3$  and MgO in the  $<2 \mu m$  fraction should vary together with the proportion of less expandable layers. This is clearly not the case (see Table 1) probably because the composition variations expected are too small to be detected by such averaging bulk chemical analyses. The distribution of tetrahedral charge may be responsible for the heterogeneous expansion behaviour observed in

intermediate- and high-charge layers after K-saturation. According to this hypothesis, the location of the layer charge may be assessed for the three layer types defined above. Low-charge smectite layers are mostly octahedrally substituted, whereas for intermediate- and high-charge layers this montmorillonitic charge is complemented by additional tetrahedral substitutions (0.30 and 0.35–0.40 charge per  $O_{10}(OH)_2$ , respectively).

#### *MLM variation throughout the profile*

In the upper part, the composition of the dominant MLM (I-Exp<sub>1</sub>) changes progressively with depth as shown by the K-saturation test and the migration of its main peak from 17.03 Å (sample E) to 16.22 Å (sample A). This indicates that the amount of high-charge layers increases towards the top of the bentonite bed. However the increased charge is not related to a significant change in the K or Al content in the bulk composition of the clay-size fraction, suggesting that the studied bentonite bed from Charente is not a K-bentonite type, where K and Al are changed by a post-deposit diffusion process (Cetin & Huff, 1995).

On the other hand, the observed change in expandability is correlated with the limited but steady CEC increase from the centre of the bentonite bed ( $\sim 74 \text{ cmol kg}^{-1}$ ) towards its edges ( $\sim 80 \text{ cmol kg}^{-1}$ , Table 2). This increase correlates with both Ca and Na contents (Fig. 3), indicating that the amount of these cations is ruled by the CEC of the expandable layers in the bentonite, and hence by the layer-charge heterogeneities. If this reasoning is correct, the mineral changes observed in the layer are due to re-adjustments in an essentially isochemical system, at least concerning the elements Mg, Al, Si, K and Fe (no visible changes in chemical compositions presented in Table 1). In this isochemical system, the evolution of hydration ability, expandability and CEC with depth in the bentonite bed must be due to different interlayer charge distributions in expandable layers. For example, for the same layer charge, octahedral and tetrahedral substituted sites may be or not superimposed inside the volume delimited by the upper and lower hexagonal cavities. As a result, the number of highly charged sites may vary: if low, the total charge is spread over the layer surface increasing the CEC and reducing the swelling ability.

## CONCLUSIONS

The studied Charente bentonite bed, although largely smectitic and containing I-S minerals, does not correspond to a K-bentonite occurrence where K and Al are exchanged for other elements during a diffusion process which gradually replaces smectite by illite layers in a sequence of I-S minerals. It is possible that the Charente bentonite corresponds to the initial stage of smectite formation from an ash layer, and that it has not been affected by the processes generating K-bentonites usually described. According to this hypothesis, it is clear that the initial clay mineralogy of the bentonite (smectite) is not homogeneous nor monophasic at any one given point. In fact the Charente bentonite shows mineralogical zoning from the edge toward the centre even though its chemistry is not zoned.

## ACKNOWLEDGMENTS

Financial support was provided by UMR 6532 of the CNRS and University of Poitiers (France). The authors thank Drs J. Cuadros and R. Dorham for their helpful comments on an early version of this manuscript and Anne-Marie Karpoff for her editorial assistance.

## REFERENCES

- Altaner S.P. (1985) *Potassium metasomatism and diffusion in Cretaceous K-bentonites from the Disturbed Belt, north-western Montana and in the Middle Devonian Tioga K-bentonite, eastern USA*. PhD thesis, University of Illinois.
- Altaner S.P., Hower J., Whitney G. & Aronson J.L. (1984) Model for K-bentonite formation: Evidence from zoned K-bentonites in the disturbed belt, Montana. *Geology*, **12**, 412–415.
- Calarge L., Lanson B., Meunier A. & Formoso M.L. (2003) The smectitic minerals in a bentonite deposit from Melo (Uruguay). *Clay Minerals*, **38**, 25–34.
- Cetin K. & Huff W.D. (1995) Layer charge of the expandable component of illite/smectite in K-bentonite as determined by alkylammonium ion exchange. *Clays and Clay Minerals*, **43**, 150–158.
- Cuadros J. & Altaner S.P. (1998) Compositional and structural features of the octahedral sheet in mixed-layer illite/smectite from bentonites. *European Journal of Mineralogy*, **10**, 111–124.
- Drits V.A., Lindgreen H., Sakharov B.A. & Salyn A.S. (1997) Sequence structure transformation of illite-smectite-vermiculite during diagenesis of Upper Jurassic shales, North sea. *Clay Minerals*, **33**, 351–371.
- Esposito K.J. & Whitney G. (1995) Thermal effects of thin igneous intrusions on diagenetic reactions in a Tertiary basin of Southwestern Washington. *US Geological Survey Bulletin*, **2085–C**, 36 pp.
- Foscolos A.E. & Kodama H. (1974) Diagenesis of clay minerals from lower Cretaceous shales of north eastern British Columbia. *Clays and Clay Minerals*, **22**, 319–335.
- Hoffman J. & Hower J. (1979) Clay mineral assemblages as low grade metamorphic geothermometers: application to the thrust faulted disturbed belt of Montana, USA. Special Publication, **26**, Society of Economic Paleontologists and Mineralogists, Tulsa, Oklahoma, pp. 55–79.
- Hofmann U. & Klemen E. (1950) Loss of exchangeability of lithium ions in bentonite on heating. *Zeitschrift für anorganische und Allgemeine Chemie*, **262**, 95–99.
- Huff W.D. & Türkmenoglu A.G. (1981) Chemical characteristics of Ordovician K-bentonites along the Cincinnati Arch. *Clays and Clay Minerals*, **29**, 113–123.
- Inoue A., Bouchet A., Velde B. & Meunier A. (1989) A convenient technique to estimate smectite layer percentage in randomly interstratified illite/smectite minerals. *Clays and Clay Minerals*, **37**, 227–234.
- Lagaly G. & Weiss A. (1969) Determination of the layer charge in mica-type layer silicates. *Proceedings of the International Clay Conference, Tokyo*, **1**, 61–80.
- Lanson B. (1997) Decomposition of experimental X-ray diffraction patterns (profile fitting): a convenient way to study clay minerals. *Clays and Clay Minerals*, **45**, 132–146.
- Meunier A., Proust D. & Moreau P. (1999) Geological significance of two smectite-rich beds from Lower Cenomanian sediments, northern Aquitaine basin, France. *Bulletin de la Société Géologique de France*, **170**, 873–882.
- Meunier A., Lanson B. & Beaufort D. (2000) Vermiculitization of smectite interfaces and illite layer growth as a possible dual model for illite-smectite illitization in diagenetic environments: a synthesis. *Clay Minerals*, **35**, 573–586.
- Moore D.M. & Reynolds R.C. (1989) *X-ray Diffraction and the Identification and Analysis of Clay Minerals*. Oxford University Press, Oxford, UK.
- Olis A.C., Malla P.B. & Douglas L.A. (1990) The rapid estimation of the layer charges of 2:1 expanding clays from a single alkylammonium ion expansion. *Clay Minerals*, **25**, 39–50.
- Plançon A. & Drits V.A. (2000) Phase analysis of clays using an expert system and calculation programs for X-ray diffraction by two- and three-component mixed-layer minerals. *Clays and Clay Minerals*, **48**, 57–62.
- Sakharov B.A., Lindgreen H., Salyn A.L. & Drits V.A. (1999) Determination of illite-smectite structures

- using multispecimen X-ray diffraction profile fitting. *Clays and Clay Minerals*, **40**, 103–113.
- Środoń J. (1981) X-ray identification of randomly interstratified illite-smectite in mixtures with discrete illite. *Clay Minerals*, **16**, 297–304.
- Šuchá V., Kraus I., Gerthofferova H., Petes J. & Serekova M. (1993) Smectite to illite conversion in bentonites and shales of the East Slovak basin. *Clay Minerals*, **28**, 243–253.
- Velde B. & Brusewitz A.M. (1982) Metasomatic and non-metasomatic low-grade metamorphism of Ordovician meta-bentonites in Sweden. *Geochimica et Cosmochimica Acta*, **46**, 446–452.
- Velde B., Suzuki T. & Nicot E. (1986) Pressure-temperature-composition of illite/smectite mixed-layer minerals: Niger delta mudstones and other examples. *Clays and Clay Minerals*, **34**, 435–441.
- Watanabe T. (1988) The structural model of illite/smectite interstratified minerals and the diagram for their identification. *Clay Science*, **7**, 97–114.
- Weir A.H., Ormerod E.G. & El Mansey I.M.I. (1975) Clay mineralogy of sediments of the western Nile Delta. *Clay Minerals*, **10**, 369–386.